QUADRATIC CONSTITUTIVE RELATION FOR A CORNER FLOW AND ITS APPLICATION TO A WING-BODY JUNCTURE FLOW

Hiroyuki Abe
Japan Aerospace Exploration Agency
Chofu, Tokyo 182-8522, Japan
abe.hiroyuki@jaxa.jp

Taisuke Nambu
Japan Aerospace Exploration Agency
Chofu, Tokyo 182-8522, Japan
nambu.taisuke@jaxa.jp

Yasuhiro Mizobuchi
Japan Aerospace Exploration Agency
Chofu, Tokyo 182-8522, Japan
mizobuchi.yasuhiro@jaxa.jp

ABSTRACT

In the present study, we have developed a quadratic constitutive relation (QCR) for a nonlinear two-equation k-ε model (AMM-QCR$_{corner}$) by focusing on the behavior of the mean streamwise vorticity in a corner flow. The present QCR consists of three terms (i.e. SΩ, SS and ΩΩ terms). Results in a square duct flow indicate that the inclusion of the ΩΩ term improves the Reynolds normal stress anisotropy near a corner and strengthens the mean streamwise vorticity there.

We have then tested AMM-QCR$_{corner}$ against the wing-body juncture flow in an airfoil (i.e. NASA Juncture Flow), where corner separation occurs in the trailing edge. In this testing, the modification is made for the expression of the turbulent eddy viscosity by introducing a parameter $S_{ij}^2-\Omega_{ij}^2$, representing the acceleration and deceleration of the mean flow. This is effective for improving the overprediction of the eddy viscosity in the trailing edge of a corner. Results highlight that AMM-QCR$_{corner}$ reproduces a separation bubble whose size is comparable to that of the experiment.

INTRODUCTION

The prediction for a corner flow (i.e. wing-body juncture flow) is one of the challenging issues in the engineering and aeronautics. While eddy viscosity models (i.e. one-equation SA (Spalart and Allmaras 1994) model and two-equation k-ω (Wilcox 1988), and SST (Menter 1994) models) are widely used in practical applications, a linear eddy viscosity does not intrinsically yield a secondary flow near a corner since the Reynolds stress anisotropy is not resolved there. In the k- ε model, Nishizima and Yoshizawa (1987) and Myong and Kasagi (1990) proposed QCRs and Craft et al. (1996) proposed a cubic constitutive relation for the eddy viscosity. On the other hand, Spalart (2000) proposed a simple QCR for the SA model (denoted as SA-QCR2000), i.e.,

$$-\overline{u_i u_j} = 2\nu_t S_{ij} - 2\nu_t C_{nl1}\left[O_{ik}S_{jk} + O_{jk}S_{ik}\right]. \qquad (1)$$

Here, $\overline{u_i u_j}$ denotes the Reynolds stress; ν_t is the turbulent eddy viscosity; a model constant C_{nl1} is equal to 0.3; $O_{ik} \equiv \left(\overline{U}_{i,k} - \overline{U}_{k,i}\right)/\sqrt{\overline{U}_{m,n}\overline{U}_{m,n}}\left(=2\Omega_{ik}/\sqrt{\overline{U}_{m,n}\overline{U}_{m,n}}\right)$, $S_{ij} \equiv \left(\overline{U}_{i,j} + \overline{U}_{j,i}\right)/2$ and $\Omega_{ij} \equiv \left(\overline{U}_{i,j} - \overline{U}_{j,i}\right)/2$ denote the mean strain and vorticity tensors; $\overline{U}_i$ represents the mean velocity; the subscript i=1,2,3 refers to the streamwise (*x*), wall-normal (*y*) and spanwise (*z*) directions, respectively. Spalart (2000) showed that Eq. (1) reproduces a secondary flow in a square duct successfully. This QCR is currently used in aeronautics for predicting a corner flow.

On the other hand, we are developing a non-linear k- ε model (the AMM model) using DNS data in wall-bounded turbulent flows with a view to predicting separated turbulent flows in the aeronautical applications (Abe, Mizobuchi and Matsuo 2019; 2020). For improving the Reynolds normal stress anisotropy, two QCRs (AMM-QCR) were developed with the use of DNS data of a turbulent separation bubble (Abe 2017), i.e.

$$\begin{aligned}-\overline{u_i u_j} = &-\frac{2}{3}k\delta_{ij} + 2\nu_t S_{ij} - C_1'\frac{\nu_t^2}{k}\left[\Omega_{ik}S_{jk} + \Omega_{jk}S_{ik}\right] \\ &- C_2'\frac{\nu_t^2}{k}\left[S_{ik}S_{kj} - \frac{1}{3}S_{mn}S_{mn}\delta_{ij}\right]\end{aligned}, \qquad (2)$$

$$\begin{aligned}-\overline{u_i u_j} = &-\frac{2}{3}k\delta_{ij} + 2\nu_t S_{ij} - C_1\frac{k}{\varepsilon}\nu_t\left[\Omega_{ik}S_{jk} + \Omega_{jk}S_{ik}\right] \\ &- C_2\frac{k}{\varepsilon}\nu_t\left[S_{ik}S_{kj} - \frac{1}{3}S_{mn}S_{mn}\delta_{ij}\right]\end{aligned} \qquad (3)$$

with $C_1' = C_2' = 3.2$ and $C_1 = C_2 = 0.6$. The application to the NASA Juncture Flow however led to a smaller corner separation bubble than that of the experiment (Abe et al. 2020). One of the reasons is most likely due to the insufficient predictions of Eqs. (2) and (3) in a corner flow.

Here, we consider the non-zero value of the mean streamwise vorticity $\overline{\Omega}_x$ in a corner flow where the Reynolds normal stress anisotropy plays a crucial role (Bradshaw 1987). We then propose a new QCR (i.e. AMM-QCR$_{corner}$) by adding a ΩΩ term to Eq. (3), i.e.

$$\begin{aligned}-\overline{u_i u_j} = &-\frac{2}{3}k\delta_{ij} + 2\nu_t S_{ij} - C_1\frac{k}{\varepsilon}\nu_t\left[\Omega_{ik}S_{jk} + \Omega_{jk}S_{ik}\right] \\ &- C_2\frac{k}{\varepsilon}\nu_t\left[S_{ik}S_{kj} - \frac{1}{3}S_{mn}S_{mn}\delta_{ij}\right] - C_3\frac{k}{\varepsilon}\nu_t\left[\Omega_{ik}\Omega_{kj} + \frac{1}{3}\Omega_{mn}\Omega_{mn}\delta_{ij}\right]\end{aligned} \qquad (4)$$

with $C_1 = 0.6, C_2 = 0.2, C_3 = -0.3$. The latter coefficients have been determined using DNS data in the channel and square duct flows.

The objective of the present study is to clarify the effect of Eq. (4) in a corner flow by comparing with those of Eqs. (1) to (3). For this purpose, we examine two corner flows. One is a square duct flow, where the predictions are evaluated against the DNS data (Pirozzoli et al. 2018). The other is NASA Juncture Flow, which is a wing-body juncture flow and involves corner separation in the trailing edge of the wing near a wing-root junction (i.e. side-of-body separation) due to the adverse pressure gradient (see Rumsey et al. 2019). For the latter flow, the measurement was made by Kegerise and Neuhart (2019) at subsonic conditions. The Reynolds number based on crank chord is 2.4 million. The Mach number is 0.189. The experimental data are available in Kegerise and Neuhart (2019), as well as on the NASA Turbulence Modeling Resource (TMR) website (https://turbmodels.larc.nasa.gov), which are compared with

the predictions by AMM-QCR$_{corner}$ (the AMM model with Eq. (4)) and SA-QCR2000 (the SA model with Eq. (1)).

AMM MODEL

The AMM model is a low *Re* k-ε model (Abe, Mizobuchi and Matsuo 2019, 2020), which is developed with a view to predicting separated turbulent flows. In this context, AKN model (Abe, Kondoh and Nagano 1994) is often used in the k-ε model, where the near-wall model functions were developed on the basis of the Kolmogorov scale. In the AMM model, the model functions are expressed as

$$f_\mu = \left\{1-\exp\left(-\frac{R_y}{120}\right)\right\}\left[1+\frac{5}{R_t^{3/4}}\exp\left\{-\left(\frac{R_t}{200}\right)^2\right\}\right], \quad (5)$$

$$f_\varepsilon = \left\{1-\exp\left(-\frac{R_y}{12}\right)\right\}\left[1-\frac{2}{9}\exp\left\{-\left(\frac{R_t}{6}\right)^2\right\}\right]. \quad (6)$$

Here, R_y is the Reynolds number based on the square-root of the turbulent kinetic energy $\sqrt{k}$ and the distance from the wall y. Eqs. (5) and (6) are applicable to separated turbulent flows. The original AMM model constants were determined using the DNS data of a turbulent channel flow, which are expressed as $C_\mu = 0.09$, $\sigma_k = \sigma_\varepsilon = 1.4$, $C_{\varepsilon_1} = 1.5$, and $C_{\varepsilon_2} = 1.9$. In the present study, we use the modified diffusion coefficients, i.e., $\sigma_k = 1.1$ and $\sigma_\varepsilon = 1.25$. These values have been obtained on the basis of the mathematical analysis of Cazalbou, Spalart and Bradshaw (1994) by Abe and Spalart (2020).

Figure 1a shows the predictions of the AMM model for the normalized mean streamwise velocity $\overline{U}$ in a turbulent channel flow at the friction Reynolds number $Re_\tau = U_\tau h/\nu = 2000$ (U_τ and h denote the friction velocity and the channel half-width, respectively). The AMM result agrees well with the DNS data (Jimenez and Hoyas 2006) as well as those of the AKN (Abe, Kondoh and Nagano 1994) and MK (Myong and Kasagi 1990) models. Figure 1b shows the predictions of the AMM model with Eqs. (2) to (4) for the Reynolds normal stresses. Equation (3) gives a better prediction for the Reynolds normal stresses than Eq. (2), and provides the prediction that $\overline{vv}$ and $\overline{ww}$ agree well with the DNS data except close to the wall, although $\overline{uu}$ is underpredicted by 30 percent there. On the other hand, Eqs. (3) and (4) yield essentially the identical behaviors, highlighting that the inclusion of the ΩΩ term in Eq. (4) does not affect the predictions for the two-dimensional wall turbulence. The difference between Eqs. (3) and (4) is however of importance for improving the predictions for a corner flow, which will be discussed in the next section.

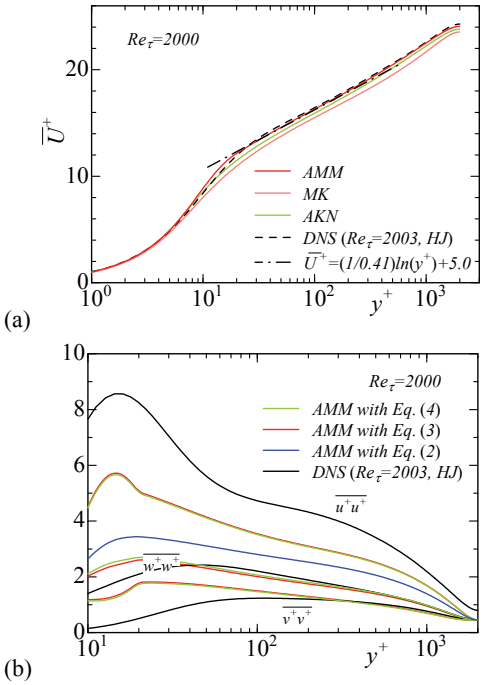

Figure 1. Predictions for normalized mean velocity $\overline{U}$ and the Reynolds normal stresses $\overline{uu}$, $\overline{vv}$, $\overline{ww}$ in a turbulent channel flow at Re_τ=2000: (a) $\overline{U}^+$; (b) $\overline{u^+u^+}$, $\overline{v^+v^+}$, $\overline{w^+w^+}$ (the superscript + denotes normalization by wall units). AMM with Eqs. (2) to (4) have been tested. Note that for AMM with Eq. (2), the $\overline{u^+u^+}$ data have been exclusively plotted (v, w components are not shown). The calculated data have been compared with the DNS data of Hoyas and Jimenez (2006).

RESULTS AND DISCUSSION

Square Duct

We first examine the predictions of AMM-QCR$_{corner}$ (Eq. (4)) in a square duct by comparing with those of the AMM model with different QCRs (i.e. Eq. (2) and (3)). The flow is driven by a constant mean pressure gradient, which is solved by an incompressible flow code with a second-order accuracy in space. The friction Reynolds number is Re_τ=1000. The number of grid points are 448 × 448 in the wall-normal (y) and spanwise (z) directions (note that the grid is clustered near the wall).

Figure 2 shows the contours in the y-z plane of the normalized mean streamwise velocity $\overline{U}$ with velocity vectors, predicted by the AMM model with Eqs. (2) to (4). Indeed, use of the QCR reproduces the secondary flow near a corner. There are however some differences in the predictions. The AMM model with Eq. (2) predicts a weaker

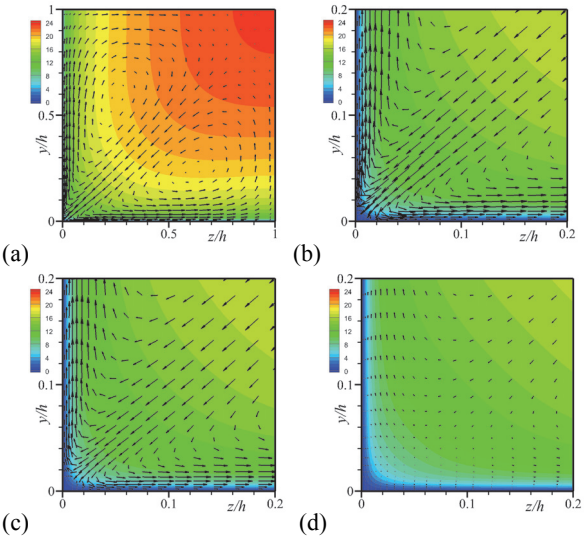

Figure 2. Contours in the y-z plane of normalized mean streamwise velocity with velocity vectors in a square duct at Re_τ=1000, calculated with AMM model using various QCRs: (a), (b) AMM with Eq. (4) (AMM-QCR$_{corner}$); (c) AMM with Eq. (3) (AMM-QCR) ; (d) AMM with Eq. (2) (AMM-QCR).

secondary flow than that with Eq. (3). This is attributed to the increased effect of the damping function f_μ in the time scale term (ν_t / k) of Eq. (2). On the other hand, the AMM model with Eq. (4) yields a stronger secondary flow than that with Eqs. (2) and (3), which is essentially owing to the effect of the ΩΩ term in Eq. (4).

Figure 3 shows the contours in the y-z plane of the normalized mean streamwise vorticity $\overline{\Omega}_x$ in a square duct near a corner. Indeed, we see a large magnitude of $\overline{\Omega}_x$ in the

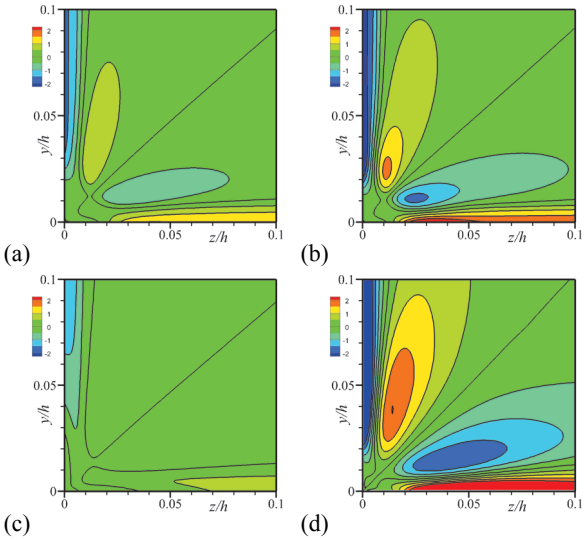

Figure 3. Distributions of $\overline{\Omega}_x$ normalized by U_b / h in a square duct for Re_τ=1000, calculated using AMM model with various QCRs; (a) AMM with Eq. (3) (AMM-QCR); (b) AMM with Eq. (4) (AMM-QCR$_{corner}$); (c) AMM with Eq. (1); (d) DNS by Pirozzoli et al. (2018) .

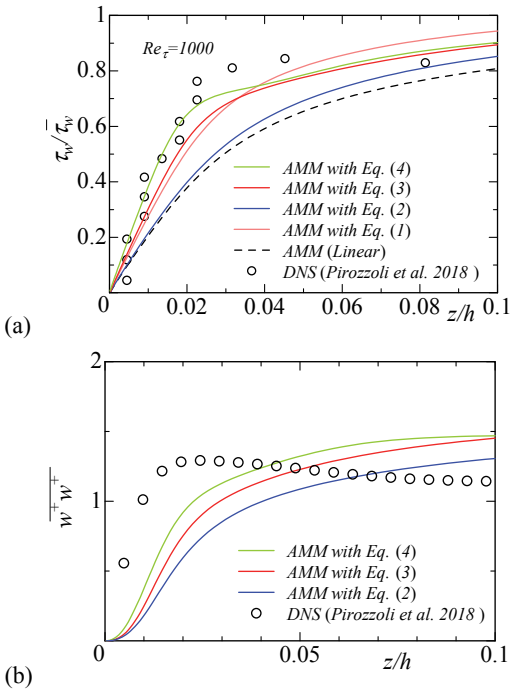

Figure 4. Normalized local wall shear stress τ_w and spanwise Reynolds normal stress in a square duct for Re_τ=1000, calculated with AMM using various QCRs. The enlarged view in the region y/h=0 to 0.1 is shown. The calculated data have been compared with the DNS data of Pirozzoli et al. (2018).

prediction of the AMM model with Eq. (4), which agrees reasonably with the DNS result by Pirozzoli et al. (2018). On the other hand, there is a weaker magnitude of $\overline{\Omega}_x$ for the prediction with Eq. (3) than that with Eq. (4), indicating that the inclusion of the ΩΩ term in Eq. (4) plays a role in strengthening the mean streamwise vorticity near a corner. Figures 3(b) and (c) show the comparison in the predictions obtained from the AMM model with Eq. (4) and that with Eq. (1), the latter QCR being widely used in the aeronautical applications. Indeed, the prediction of the AMM model with Eq. (4) (AMM-QCR$_{corner}$) yields a larger magnitude of $\overline{\Omega}_x$ than AMM with Eq. (1).

An inspection revealed that the predictions of the AMM model with Eq. (4) for $\overline{vv}$ (not shown here) and $\overline{ww}$ (figure 4b) are closer to the DNS data than those with the AMM model with Eq. (3), indicating that the Reynolds normal stress anisotropy is improved in Eq. (4). This is due to the term $C_3(k/\varepsilon)\nu_t\Omega_{32}\Omega_{32} = -C_3(k/\varepsilon)\nu_t\overline{\Omega}_x^2 > 0$ in Eq. (4).

Figure 4 shows the normalized wall shear stress τ_w in a square duct near a corner at y/h=0.01. Indeed, the AMM model with Eq. (4) leads to a larger magnitude of τ_w . The latter distribution agrees well with the DNS data of Pirozzoli et al. (2018). This result highlights the importance of including the ΩΩ term in the QCR for improving the prediction in a corner flow.

NASA Juncture Flow

We next examine the predictions for the NASA Juncture Flow (JF) with a hone. The full span JF model consists of a fuselage and two wings, where the wing span is 3397.250 mm, and the fuselage length is 4839.233 mm (see the details in Rumsey et al. 2019). In this flow, a separation bubble (i.e. side-of-body separation) occurs near the trailing edge of the wing near a wing-root junction where the adverse pressure gradient is large. We thus need to predict not only a separated flow but also a secondary flow induced by the Reynolds stress as accurately as possible. It was noted that the prediction with a linear eddy viscosity model yields a larger separation bubble near a corner, while use of the QCR reduces the size of the separation bubble (see Yamamoto et al. 2012). Particular attention is therefore given to the prediction for the corner separation bubble with the QCR.

The flow solver used in the present study is FaSTAR developed by JAXA (Hashimoto et al. 2012), which is an unstructured-grid compressible flow solver with the second-order accuracy. The inviscid flux scheme HLLEW (Obayashi and Guruswamy 1995) is used for the convective terms. The numerical flux has been calculated at a cell vertex. The details on the numerical methodology are given in Hashimoto et al. (2012).

The grids used in the present study are those provided by the TMR website (https://turbmodels.larc.nasa.gov). The grid dependency on the JF computation with the AMM model has been examined by Abe et al. (2020) using three unstructured grids for free-air (i.e. without considering the mast and sting support system), where the number of grid points are 12,312,544 (coase), 39,121,991 (MED) and 160,761,294 (FINE). It was shown that the difference in the predictions between the coarse and MED grids is greater than that between the MED and FINE grids. In the present study, we therefore use two grids, i.e. coarse and MED grids for clarifying the effect of the QCR on the prediction of a corner separation bubble. Referring to the comprehensive study of

Spalart and Rumsey (2009), the turbulence intensity T_u and the viscous ratio ν_t/ν for the AMM model is 0.08 and 0.1. The attack of angles computed in the present study are in the range α= -2.5 to 5 °.

As noted in the introduction, our earlier study in this flow (Abe et al. 2020) reported that a smaller corner separation bubble is predicted compared with that of the experiment when the AMM model with Eq. (3) is used. A close inspection revealed that this is intrinsically associated with the overestimation of the eddy viscosity when the adverse pressure gradient is large (see the contours of ν_t in Fig. 7b). In the current study, we therefore modify the expression for ν_t by incorporating a parameter $S_{ij}^2-\Omega_{ij}^2$, representing the acceleration and deceleration of the mean flow, into the turbulence time scale T_μ using the augmented time scale procedure by Yoshizawa et al. (2006), i.e.,

$$\nu_t = C_\mu f_\mu k T_\mu \Big/ \left(1+C_{SO}\left[\left(S_{ij}^2-\Omega_{ij}^2\right)\left(k/\varepsilon\right)^2\right]^2\right)^{1/2}, \quad (7)$$

where C_{SO} is a model constant. The value of C_{SO}=1 is used after testing the values of 0.5, 1 and 2 in the current flow. We also modify the near-wall behavior in the diffusion coefficients as follows, i.e.,

$$\sigma_k = 1.1/f_{sig} \text{ and } \sigma_\varepsilon = 1.25/f_{sig}, \quad (8)$$

where

$$f_{sig} = 1+6\left(-\exp\left(R_y/20\right)^2\right) . \quad (9)$$

Other modification is the realizability limiter. We use that proposed by Medic and Durbin (2002) on turbine blades, i.e.

$$T_\mu = \min\left(\frac{k}{\varepsilon}, \frac{0.6}{\sqrt{6}C_\mu\left(S_{ij}^2\right)^{1/2}}\right). \quad (10)$$

The value of the numerator (=0.6) in Eq. (10) is smaller than that (=1.0) of the original limier in the AMM model (see Abe et al. 2020). This modification is done by considering computations for practical applications.

Figure 6 shows the predictions of AMM-QCR$_{corner}$ with/without the modification of Eq. (7) for the skin friction coefficient C_f and the streamlines. Also shown in Figure 7 are the contours of ν_t in the trailing edge of the wing near a corner. The attack of angle is α= 5 °. The coarse grid is used. When the original eddy viscosity expression $\nu_t = C_\mu f_\mu k T_\mu$ is used (Figs. 6b and 7b), the magnitude of ν_t becomes large in the trailing edge of the wing-body juncture so that the separation bubble predicted is approximately twice smaller than that of the experiment. Use of Eq. (7) indeed improves the prediction near a corner where the magnitude of ν_t becomes smaller than the prediction with $\nu_t = C_\mu f_\mu k T_\mu$ so that the size of the separation bubble is comparable to that of the experiment. This result underlines that Eq. (7) is effective for improving the overprediction of ν_t in the trailing edge near a corner and yielding a larger size of the separation bubble; $S_{ij}^2-\Omega_{ij}^2$ is an important parameter for characterizing turbulent flows with a mean pressure gradient.

Figure 8 shows the enlarged view of the corner separation bubble, predicted by the AMM, AMM-QCR$_{corner}$ and SA-QCR2000 (noft2) models at α= 5 °. The MED grid is used. When a linear model (i.e. the AMM model) is used, there appears a large separation bubble near a corner. Use of the QCR (i.e. the AMM-QCR$_{corner}$ model) reduces the size of the corner separation bubble (see Figs. 8a and b; see also Table 1 where the size of the bubble is compared with that of experiment). This behavior is consistent with that of Yamamoto et al. (2012) on the NASA CRM wing-body computations. A comparison between AMM-QCR$_{corner}$ and

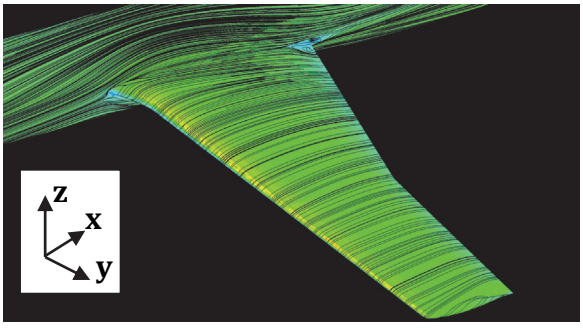

(a)

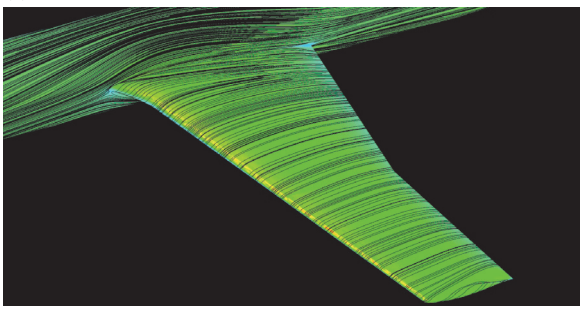

(b)

Figure 6. Contours of the skin friction coefficient C_f (color) and streamlines (black line) for AMM-QCRcorner, obtained with the attack of angle α= 5 ° and the coarse grid: (a) Eq. (7) is used for ν_t ; (b) $\nu_t = C_\mu f_\mu k T_\mu$ is used for ν_t .

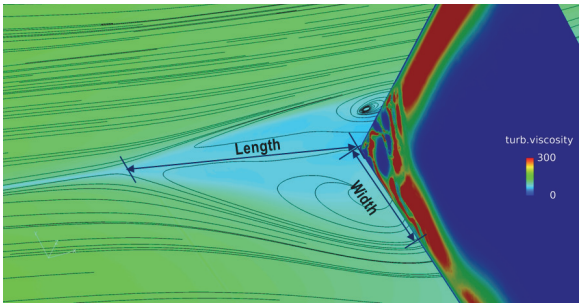

(a)

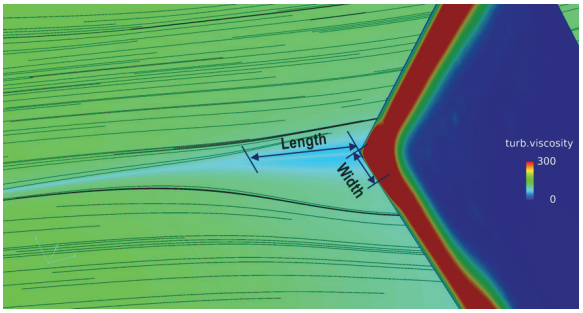

(b)

Figure 7. Contours of the skin friction coefficient C_f (color), streamlines (black line) near a corner together with those of ν_t for AMM-QCR$_{corner}$, obtained with the attack of angle α= 5 ° degrees and the coarse grid: (a) Eq. (7) is used for ν_t ; (b) $\nu_t = C_\mu f_\mu k T_\mu$ is used for ν_t .

SA-QCR2000 (Figs. 8b and c) indicates that AMM-QCR$_{corner}$ yields a smaller separation bubble than SA-QCR2000, the former model predicting a larger $\overline{\Omega}_x$ near a corner where AMM QCR$_{corner}$ reproduces a stronger secondary flow than SA-QCR2000 (see Fig. 9). This behavior is consistent with that observed in a square duct (see Fig. 3). In the wing-body juncture, the C_p distribution for AMM-QCR$_{corner}$ also agrees well with the experimental data (see Fig. 10 where AMM QCR$_{corner}$ predicts better than AMM and SA-QCR2000). An inspection indicates that the size of the bubble for AMM-QCR$_{corner}$ with α=5 is within 10 percent of the experimental results (see Table 1).

Figure 11 shows the distributions of the bubble length L and width W as a function of α. Indeed, AMM-QCR$_{corner}$ predicts W and L reasonably at each α, where the rate of increase for both W and L agrees well with that of the

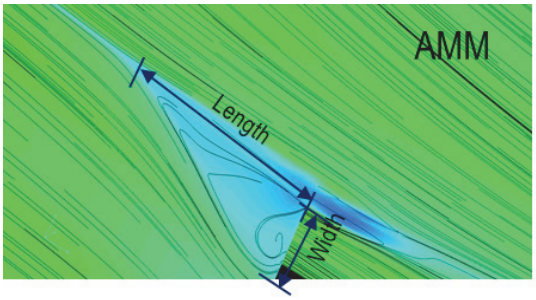

(a)

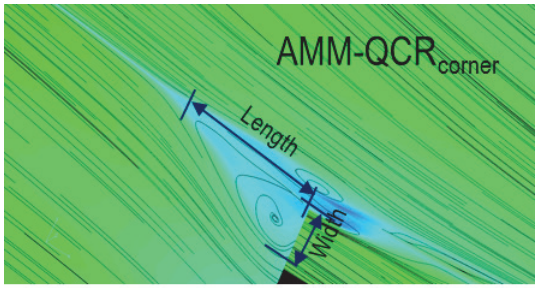

(b)

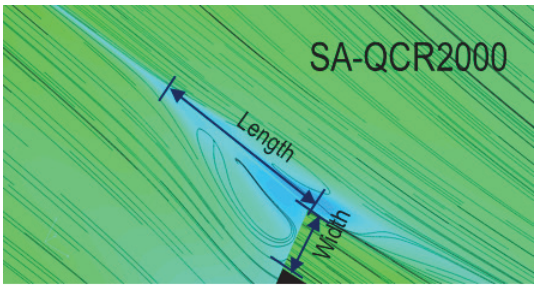

(c)

Figure 8. Contours of the skin friction coefficient C_f (color) and streamlines (black line) near a corner, obtained with the attack of angle $\alpha = 5^\circ$ and the MED grid: (a) AMM ; (b) AMM-QCR$_{corner}$; (c) SA-QCR2000. For AMM and AMM-QCR$_{corner}$, Eq. (7) is used for ν_t .

Table 1. The size of the corner separation bubble at α=5 °, obtained with the MED grid.

	Length	Width
Experiment (Error bar)	119mm (±15.5mm)	43mm (±6.8mm)
AMM-QCR$_{corner}$	129mm	47mm
AMM	173mm	71mm
SA-QCR2000	146mm	52mm

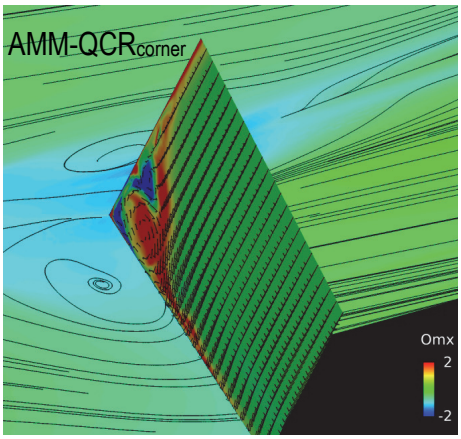

(a)

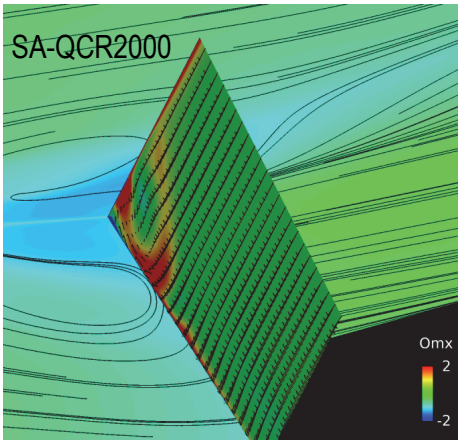

(b)

Figure 9. Contours of the skin friction coefficient C_f (color) and streamlines (black line) together with those of the mean streamwise vorticity $\overline{\Omega}_x$ and the velocity vectors near a corner for AMM, AMM-QCR$_{corner}$ and SA-QCR2000, obtained with the attack of angle $\alpha = 5^\circ$ and the MED grid: (a) AMM-QCR$_{corner}$; (b) SA-QCR2000. For AMM-QCR$_{corner}$, Eq. (7) is used for ν_t .

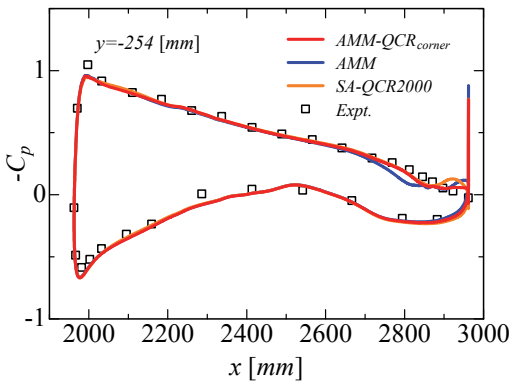

Figure 10. Distributions of the wall-pressure coefficient C_p at y=-254 mm with $\alpha = 5^\circ$ for AMM, AMM-QCR$_{corner}$ and SA-QCR2000, obtained with the MED grid.

experiment. In particular, AMM-QCR$_{corner}$ predicts L better than SA-QCR2000, highlighting the usefulness of Eq. (4) in predicting the corner separation bubble.

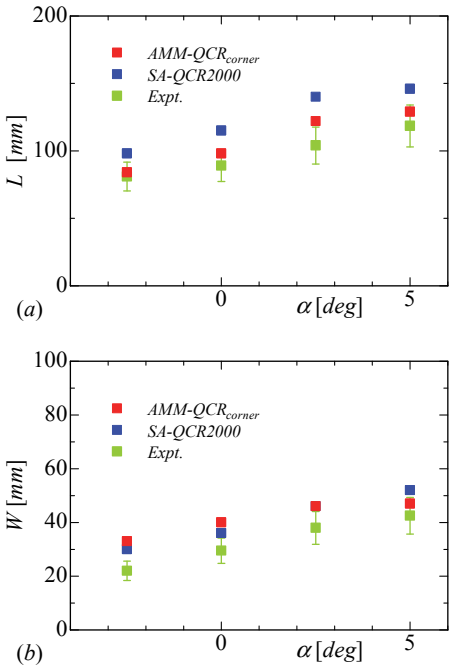

Figure 11. Distributions of the bubble length L and width W for AMM-QCR$_{corner}$ compared with those for SA-QCR2000 and the experimental data: (a) distributions of L as a function of α ; (b) distributions of W as a function of α . The experimental data of Kegerise and Neuhart (2019) are also plotted for comparison.

CONCLUSIONS

The main conclusions are summarized as follows.

1) We have developed a new QCR (Eq. 4) by considering the non-zero value of $\overline{\Omega}_x$ in a corner flow.
2) In a square duct, AMM-QCR$_{corner}$ (AMM with Eq. (4)) reproduces a strong secondary flow near a corner with large $\overline{\Omega}_x$, and the prediction agrees reasonably well with the DNS data.
3) In NASA Juncture Flow, Eq. (7) is effective for improving the overprediction of ν_t in the trailing edge near a corner. Use of the QCR reduces the size of the corner separation bubble and yields a better prediction than without QCR. Indeed, AMM-QCR$_{corner}$ (AMM with Eq. (4)) predicts a corner separation bubble whose size is comparable to that of the experiment.

REFERENCES

Abe, H., 2017, "Reynolds-number dependence of wall-pressure fluctuations in a pressure-induced turbulent separation bubble," J. Fluid Mech., Vol. 833, pp. 563–598.

Abe, H., Mizobuchi Y. and Matsuo, Y., 2019, "Prediction of turbulent flow around an airfoil with a nonlinear k-ε model," Proc. of 51th Fluid Dynamics Conference / 37th Aerospace Numerical Simulation Symposium, 2E07 (in Japanese).

Abe, H., Mizobuchi, Y. and Matsuo, Y., 2020, "Effect of a Quadratic Constitutive Relation on Juncture Flow Computations," AIAA paper 2020-2752.

Abe, K., Kondoh, T. and Nagano, Y., 1994, "A new turbulence model for predicting fluid flow and heat transfer in separating and reattaching flows–I. Flow field calculations," Int. J. Heat Mass Transfer, Vol. 37, pp. 139–151.

Abe, H. and Spalart, P. R., 2020 "Outer edge behavior of the k-ε model in a turbulent boundary layer and a new improvement to the AMM model," in preparation.

Bradshaw, P., 1987, "Turbulent Secondary Flows," Annual Review of Fluid Mech., Vol. 19, pp. 53–74

Cazalbou, J. B., Spalart, P. R. and Bradshaw, P., "On the behavior of two-equation models at the edge of a turbulent region," Phys. Fluids, Vol. 6(5), 1994, pp. 1797-1804.

Craft, T., Launder, B. and Suga, K., 1996, "Development and application of a cubic eddy-viscosity model of turbulence.," Int. J. Heat Fluid Flow, Vol. 17, pp. 108–115.

Hashimoto, A., Murakami, K., Aoyama, T., Ishiko, K., Hishida, M., Sakashita, M. and Lahur, P. R., 2012, "Toward the Fastest Unstructured CFD Code 'FaSTAR'," AIAA paper 2012-1075.

Hoyas, S. and Jiménez, J., 2006, "Scaling of the velocity fluctuations in turbulent channels up to Re_τ=2003," Phys. Fluids, Vol. 18, 011702.

Kegerise, M. A. and Neuhart, D. H., 2019, "An experimental investigation of a wing-fuselage junction model in the NASA Langley 14- by 22-foot subsonic tunnel," NASA/TM-2019-220286.

Medic, G. and Durbin, P., 2002, "Toward improved prediction of heat transfer on turbine blades," J. Turbomach., Vol. 124, pp. 187–192.

Menter, F. R., 1994, "Two-equation eddy-viscosity turbulence models for engineering applications," AIAA J., Vol. 32 (8), pp. 1598–1605.

Myong, H. and Kasagi, N., 1990, "Prediction of anisotropy of the near-wall turbulence with an anisotropic low-Reynolds-number k–ε turbulence model," J. Fluids Eng., Vol. 112, pp. 521–524.

Nisizima, S. and Yoshizawa, A., 1987, "Turbulent channel and Couette flows using an anisotropic k–ε model," AIAA J., Vol. 25, pp. 414–420.

Obayashi, S. and Guruswamy, G. P., 1995, "Convergence Acceleration of a Navier-Stokes Solver for Efficient Static Aeroelastic Computation," AIAA Journal, Vol. 33, No. 6, pp.1134–1141.

Pirozzoli, S., Modesti, D., Orlandi, P. and Grasso, F., 2018, Turbulence and secondary motions in square duct flow, J. Fluid Mech., Vol. 840, pp. 631–655.

Rumsey, C. L., Carlson, J.-R. and Ahmad, N.N., 2019, "FUN3D Juncture Flow Computations Compared with Experimental Data," AIAA paper 2019-0079.

Spalart, P. R., 2000, "Strategies for turbulence modelling and simulations," Int. J. Heat and Fluid Flow, Vol. 21, pp. 252–263.

Spalart, P. R. and Allmaras, S. R., 1994, "A One-equation turbulence model for aerodynamic flows," La Rech. Aérospatiale, Vol. 1, pp. 5–21.

Spalart, P. R. and Rumsey, C. L., 2012, "Effective Inflow Conditions for Turbulence Models in Aerodynamic Calculations," AIAA J., Vol. 45, pp. 2544-2553.

Wilcox, D. C., 1988, "Reassessment of the scale-determining equation for advanced turbulence models," AIAA J., Vol. 26(11), pp. 1299–1310

Yamamoto, K., Tanaka, K. and Murayama, M., 2012, "Effect of a nonlinear constitutive relation for turbulence modeling on predicting flow separation at wing-body juncture of transonic commercial aircraft," AIAA paper 2012-2895.

Yoshizawa, A., Nisizima, S., Shimomura, Y., Kobayashi, H., Matsuo, Y., Abe, H. and Fujiwara, H., 2006, "A new methodology for Reynolds-averaged modeling based on the amalgamation of heuristic-modeling and turbulence-theory methods," Phys. Fluids, Vol. 18, 035109.

ACKNOWLEGDEMENTS

Computations performed on the JAXA Supercomputer System are gratefully acknowledged. HA would like to thank Prof. Y. Matsuo for the earlier collaboration, Drs. P. R. Spalart and K. Yamamoto for the discussion on the QCRs and Dr. M. Hishida and Mr. K. Hayashi for their computational support throughout this work.